

University of Massachusetts Medical School

eScholarship@UMMS

University of Massachusetts Medical School Faculty Publications

2020-07-14

JNK-mediated disruption of bile acid homeostasis promotes intrahepatic cholangiocarcinoma


Elisa Manieri

National Centre for Cardiovascular Research, Spain

Et al.

Let us know how access to this document benefits you.

Follow this and additional works at: https://escholarship.umassmed.edu/faculty_pubs

 Part of the [Amino Acids, Peptides, and Proteins Commons](#), [Biochemical Phenomena, Metabolism, and Nutrition Commons](#), [Cancer Biology Commons](#), [Cell Biology Commons](#), [Cellular and Molecular Physiology Commons](#), [Enzymes and Coenzymes Commons](#), [Lipids Commons](#), [Molecular Biology Commons](#), [Nutritional and Metabolic Diseases Commons](#), and the [Physiological Processes Commons](#)

Repository Citation

Manieri E, Barrett T, Cavanagh-Kyros J, Davis RJ, Mora A, Sabio G. (2020). JNK-mediated disruption of bile acid homeostasis promotes intrahepatic cholangiocarcinoma. University of Massachusetts Medical School Faculty Publications. <https://doi.org/10.1073/pnas.2002672117>. Retrieved from https://escholarship.umassmed.edu/faculty_pubs/1724

Creative Commons License



This work is licensed under a [Creative Commons Attribution-NonCommercial-No Derivative Works 4.0 License](#). This material is brought to you by eScholarship@UMMS. It has been accepted for inclusion in University of Massachusetts Medical School Faculty Publications by an authorized administrator of eScholarship@UMMS. For more information, please contact Lisa.Palmer@umassmed.edu.



JNK-mediated disruption of bile acid homeostasis promotes intrahepatic cholangiocarcinoma

Elisa Manieri^{a,b,1}, Cintia Folgueira^a, María Elena Rodríguez^a, Luis Leiva-Vega^a, Laura Esteban-Lafuente^a, Chaobo Chen^c, Francisco Javier Cubero^c, Tamera Barrett^d, Julie Cavanagh-Kyros^d, Davide Seruggia^e, Alejandro Rosell^a, Fátima Sanchez-Cabo^a, Manuel Jose Gómez^a, María J. Monte^f, Jose J. G. Marin^f, Roger J. Davis^{d,2}, Alfonso Mora^{a,2}, and Guadalupe Sabio^{a,2}

^aCentro Nacional de Investigaciones Cardiovasculares, Myocardial Pathophysiology Area, 28029 Madrid, Spain; ^bDepartment of Immunology and Oncology, Centro Nacional de Biotecnología, Consejo Superior de Investigaciones Científicas, 28049 Madrid, Spain; ^cDepartment of Immunology, Ophthalmology, and ENT, Complutense University School of Medicine, 28040 Madrid, Spain; ^dProgram in Molecular Medicine, University of Massachusetts Medical School, Worcester, MA 01605; ^eDivision of Hematology/Oncology, Boston Children's Hospital, Dana-Farber Cancer Institute, Harvard Medical School, Boston, MA 02215; and ^fLaboratory of Experimental Hepatology and Drug Targeting, National Institute for Study of Liver and Gastrointestinal Diseases (CIBERehd), University of Salamanca, 37007 Salamanca, Spain

Contributed by Roger J. Davis, May 14, 2020 (sent for review February 12, 2020; reviewed by Anton M. Bennett and J. Silvio Gutkind)

Metabolic stress causes activation of the cJun NH₂-terminal kinase (JNK) signal transduction pathway. It is established that one consequence of JNK activation is the development of insulin resistance and hepatic steatosis through inhibition of the transcription factor PPAR α . Indeed, JNK1/2 deficiency in hepatocytes protects against the development of steatosis, suggesting that JNK inhibition represents a possible treatment for this disease. However, the long-term consequences of JNK inhibition have not been evaluated. Here we demonstrate that hepatic JNK controls bile acid production. We found that hepatic JNK deficiency alters cholesterol metabolism and bile acid synthesis, conjugation, and transport, resulting in cholestasis, increased cholangiocyte proliferation, and intrahepatic cholangiocarcinoma. Gene ablation studies confirmed that PPAR α mediated these effects of JNK in hepatocytes. This analysis highlights potential consequences of long-term use of JNK inhibitors for the treatment of metabolic syndrome.

JNK | PPAR α | bile acid | cholangiocarcinoma

Liver cancer is the fifth most common cancer and the second leading cause of cancer deaths worldwide (1, 2). Cholangiocarcinoma the second most common liver cancer, is a malignancy of bile duct epithelia with a clinically silent development and an increasing global incidence (3). Due to the absence of early markers for its diagnosis, most cholangiocarcinoma patients are identified at an advanced stage and die of metastasis (4).

Hepatic cJun NH₂-terminal kinase (JNK) has been identified as a signal transduction pathway that is critically required for obesity-induced insulin resistance and hepatic steatosis (5, 6). Indeed, mice with hepatocyte-specific JNK deficiency are resistant to high-fat diet-induced insulin resistance and steatosis (7); therefore, this signaling pathway represents a potential target for therapeutic intervention. Biochemical studies demonstrate that JNK suppresses Peroxisome Proliferator-activated Receptor α (PPAR α) activation in hepatocytes, affecting lipid metabolism and steatosis through the hepatokine FGF21 (encoded by a PPAR α target gene) (7, 8).

The transcription factor PPAR α plays a pivotal role in intracellular free fatty acid and triglyceride metabolism by regulating genes involved in fatty acid transport and degradation in mitochondria and peroxisomes (9–11). PPAR α is expressed primarily in liver, heart, and muscle and is a major regulator of fatty acid transport, catabolism, and energy homeostasis (12). PPAR α activation in the liver is increased in metabolic diseases and obesity (12), and PPAR α agonists appear to be therapeutically beneficial for the treatment of metabolic syndrome. Indeed, PPAR α activity protects against steatosis in the mouse (13) and suppresses hepatic inflammation (14). However, long-term studies in rodents showed an association of PPAR α agonists with hepatic carcinogenesis (15). These findings conflict with the growth inhibitory effects reported for PPAR α agonists in

cancer cell lines, including liver cancer cell lines (16–18). PPAR α may therefore cause context-specific actions on liver cancer development.

The activation of PPAR α modifies bile acid (BA) synthesis, conjugation, and transport (19). This change in BA metabolism can protect against steatosis, but may also promote liver cancer. An example is represented by fibroblast growth factor 15/19 (FGF15/19) that is expressed in the liver during the development of hepatocellular carcinoma and intrahepatic cholangiocarcinoma (20, 21). Notably, FGF15/19 improves glycemic responses and reduces hepatic steatosis, but also promotes liver cancer (22). These functions of BAs prompted us to examine whether long-term blockade of JNK signaling in hepatocytes, and the resulting activation of PPAR α , could alter BA homeostasis and promote liver disease.

Significance

Obesity is associated with hepatic steatosis and activation of the cJun NH₂-terminal kinase (JNK) stress-signaling pathway. Studies in mice demonstrate that JNK deficiency in the liver prevents the development of hepatic steatosis. This observation suggests that inhibition of JNK signaling may represent a possible treatment for hepatic steatosis. However, the long-term consequences of JNK inhibition are poorly understood. Here we demonstrate that loss of JNK causes changes in cholesterol and bile acid metabolism that promote cholestasis, bile duct proliferation, and intrahepatic cholangiocarcinoma. We identify PPAR α activation as the molecular mechanism that accounts for this phenotype. Our analysis has important implications for the long-term use of JNK inhibitors for the treatment of obesity.

Author contributions: R.J.D., A.M., and G.S. designed research; E.M., C.F., M.E.R., L.L.-V., L.E.-L., C.C., F.J.C., T.B., J.C.-K., D.S., A.R., F.S.-C., M.J.G., M.J.M., J.J.G.M., A.M., and G.S. performed research; E.M., C.F., F.J.C., A.R., F.S.-C., M.J.G., M.J.M., J.J.G.M., R.J.D., A.M., and G.S. analyzed data; and E.M., R.J.D., A.M., and G.S. wrote the paper.

Reviewers: A.M.B., Yale University School of Medicine; and J.S.G., University of California San Diego Medical Center.

The authors declare no competing interest.

This open access article is distributed under [Creative Commons Attribution-NonCommercial-NoDerivatives License 4.0 \(CC BY-NC-ND\)](https://creativecommons.org/licenses/by-nc-nd/4.0/).

Data deposition: The RNA-seq analysis (Fig. S2) was performed using a dataset that we have previously published (7) that was deposited in the GEO database ([GSE55190](https://www.ncbi.nlm.nih.gov/geo/query/acc.cgi?acc=GSE55190)).

¹Present address: Department of Medical Oncology and Center for Functional Cancer Epigenetics, Dana-Farber Cancer Institute, Harvard Medical School, Boston, MA 02215.

²To whom correspondence may be addressed. Email: roger.davis@umassmed.edu, amora@cnic.es, or guadalupe.sabio@cnic.es.

This article contains supporting information online at <https://www.pnas.org/lookup/suppl/doi:10.1073/pnas.2002672117/-DCSupplemental>.

First published June 29, 2020.

Results

Hepatic JNK Deficiency Alters Bile Acid Homeostasis. We have previously shown that hepatic JNK deficiency results in the activation of the transcription factor PPAR α and causes protection against diet-induced insulin resistance and hepatic steatosis (7). The activation of PPAR α may cause altered BA metabolism (19). We therefore examined BA in hepatic JNK1 plus JNK2-deficient mice (L^{DKO}) and control mice (L^{WT}) at 6 mo of age. We found that the total BA concentration in the blood of L^{DKO} mice was significantly increased compared with L^{WT} mice (Fig. 1A). The increase in circulating BA concentration is consistent with the possibility that L^{DKO} mice exhibit cholestasis.

Analysis of bile collected from the gall bladder of L^{DKO} and L^{WT} mice revealed significantly increased amounts of BA relative to the amount of cholesterol and phosphatidylcholine (PC) (Fig. 1B). Hepatic expression of genes related to hepatic PC synthesis (*Scd2*, *Chpt1*, and *Chkb*) or hepatocyte-mediated transport of PC (*Abc4* and *Atp8b1*) and BA (*Abc11* and *Slc10a1*) was markedly increased in L^{DKO} mice (SI Appendix, Fig. S1A and B). Similarly, increased expression of genes related to cholesterol synthesis (*Hmgcs1*, *Hmgcr*) and BA synthesis (*Baat*, *Cyp8b1* and *Cyp27a*) was detected in L^{DKO} mice (Fig. 1C). These data are consistent with altered biosynthesis and secretion of both cholesterol and BA through PPAR α activation.

Hepatic JNK Deficiency Causes Cholestasis and Liver Damage. It is established that cholangitis is a major risk factor for the development of cholangiocarcinoma (23). We therefore examined the liver of mature adult L^{DKO} and L^{WT} mice. No evidence of hepatic disease was found in L^{WT} mice. Similarly, analysis of hepatic sections prepared from young adult L^{DKO} mice (age 4 mo) did not indicate the presence of liver pathology (SI Appendix, Fig. S1C). However, at age 10 mo, 82% of L^{DKO} mice displayed multifocal bile duct hyperplasia together with fibrosis and inflammatory cell infiltrates (Fig. 1D). Cholangiocytes stained positively with PCNA (proliferating cell nuclear antigen), a marker for proliferation (Fig. 1D). These changes were associated with increased expression of myeloid genes (*Cd68* and *Lyz*) and inflammatory cytokines (*Ifng*, *Tnf*, *Il10*, and *Il12a*) in the liver (Fig. 1E) and increased liver damage, as monitored by the high levels of liver enzymes (ALT, AST, and γ -GT) in the blood of L^{DKO} mice (Fig. 1F). The remaining L^{DKO} mice exhibited intrahepatic cholangiocarcinoma (6%) or appeared to be healthy (12%). At age 14 mo, 95% of L^{DKO} mice displayed intrahepatic cholangiocarcinoma (Fig. 2A) associated with fibrosis (Fig. 2B) and a large increase in liver mass together with significant increases in serum levels of ALT and AST (Fig. 2C). The remaining L^{DKO} mice (6%) exhibited cystic livers with bile duct hyperplasia. Histological analysis indicated increased staining for glutamine synthetase (GS) in liver tumor lesions, together with neoplastic nodules with positive staining of the ductular markers CK19 and Sox9 (Fig. 2D). Together, these data confirm that the majority of mature mice with compound deficiency of JNK1 and JNK2 progressively develop intrahepatic cholangiocarcinoma.

The development of bile duct hyperplasia and intrahepatic cholangiocarcinoma in L^{DKO} mice was associated with increased hepatic expression of *Cytokeratin 19* (*Krt19*), a cholangiocyte-specific epithelial marker, together with the G protein-coupled BA receptor 1 (*Gpbar1*) and the apical sodium-dependent BA transporter (*Slc10a2*) that are expressed in cholangiocytes (24, 25) (Fig. 3A). The Notch receptor ligand *Jagged-1* promotes the formation of intrahepatic bile ducts (26) and was overexpressed in the liver of L^{DKO} mice (Fig. 3A). Moreover, bone morphogenetic protein 4 (*Bmp4*) mediates cholestasis-induced fibrosis (27) and cooperates with FGF to promote the development of cholangiocytes from hepatoblasts (28); expression of hepatic *Bmp4* was increased in L^{DKO} mice compared with L^{WT} mice

(Fig. 3A). Hepatoblasts can differentiate to cholangiocytes through activation of the ERK pathway (29), and BA can increase proliferation by ERK activation through the FXR/FGF15/FGFR4 pathway (30). We evaluated this pathway in mice, before cancer has developed. In concordance with elevated BA production, we found increased Farnesoid X receptor (FXR) activity, as monitored by high levels of FXR target gene (*Shp* and *Fgfr4*) expression, in L^{DKO} mice (Fig. 3B). Moreover, while control mice did not express *Fgf15*, we could detect *Fgf15* mRNA (messenger RNA) in L^{DKO} livers (Fig. 3B). Moreover, histological analysis indicated increased staining of phospho-ERK in cholangiocytes from L^{DKO} mice compared with L^{WT} mice (Fig. 3C). The increased phospho-ERK in cholangiocytes, but not hepatocytes, was confirmed by immunoblot analysis (Fig. 3D). Together, these changes in FXR/FGF15/FGFR4/ERK pathway activity may contribute to cholangiocyte proliferation and maturation from hepatoblasts, resulting in bile duct hyperplasia and the development of cholangiocarcinoma detected in L^{DKO} mice.

PPAR α Deficiency Reduces Liver Cancer in JNK1/2 Deficient Liver. We examined hepatic gene expression in chow-fed WT and L^{DKO} mice using RNA-seq data (7) and found evidence for activation of PPAR α and FXR transcription factors in the liver of L^{DKO} mice compared to L^{WT} mice (SI Appendix, Fig. S2). To test the role of PPAR α , we ablated the *Ppara* gene in L^{DKO} mice to examine whether PPAR α is required for the development of intrahepatic cholangiocarcinoma. PPAR α plus JNK1/2 liver-deficient mice (L^{PPAR α DKO}) exhibited reduced tumor burden and tumor incidence compared with L^{DKO} mice (Fig. 4A). The major changes in BA were also reversed (Fig. 4B). This is consistent with reduced hepatic expression in L^{PPAR α DKO} mice of genes involved in cholesterol and BA synthesis (*Hmgcr*, *Baat*, *Cyp8b1*, and *Cyp27a*) and hepatocyte-mediated BA transport (*Abc11*, *Abc4*, *Abcg5*, *Abcg8*) (Fig. 4C). Histological analyses indicated that PPAR α deficiency caused increased liver steatosis, but reduced hallmarks of carcinogenesis (anisokaryosis, apoptosis, ductogenesis, dysplasia, and mitosis) in L^{PPAR α DKO} compared with L^{DKO} mice (Table 1 and Fig. 4D). Moreover, CK19 and SOX9 staining were increased in L^{DKO} mice compared with L^{PPAR α DKO}, consistent with cholangiocyte proliferation. Furthermore, the prominent staining for GS by liver tumor lesions in L^{DKO} mice was suppressed in the liver of L^{PPAR α DKO} mice (Fig. 4D).

Gene expression analysis demonstrated that both inflammation and cholangiocarcinoma markers were reduced in L^{PPAR α DKO} mice compared with L^{DKO} mice (Fig. 5A and B). This evidence suggests that PPAR α deficiency protected against the promotion of cholangiocyte proliferation in mice lacking hepatocyte JNK1/2. To evaluate whether PPAR α deficiency and subsequent normalization of BA production blunted the FXR/FGF15/FGFR4/ERK pathway, we evaluated FXR target gene expression. We found that hepatic expression of *Fgf15* and *Shp* was reduced in L^{PPAR α DKO} mice compared with L^{DKO} mice (Fig. 5C). Indeed, immunoblot analysis confirmed that PPAR α deficiency suppressed the increased FGF15/21 expression detected in JNK-deficient cholangiocytes (Fig. 5D). This is consistent with the observation of lower levels of ERK activation, detected by immunohistochemistry, in L^{PPAR α DKO} cholangiocytes (Fig. 5E).

Discussion

Since increased BA can lead to inflammation, apoptosis, and necrosis of hepatocytes (31, 32), long-term elevated BA levels in patients are considered a risk factor for liver cancer development (33). Indeed, serum BA might be useful for the diagnosis of cholangiocarcinoma (34). Our findings provide an animal model

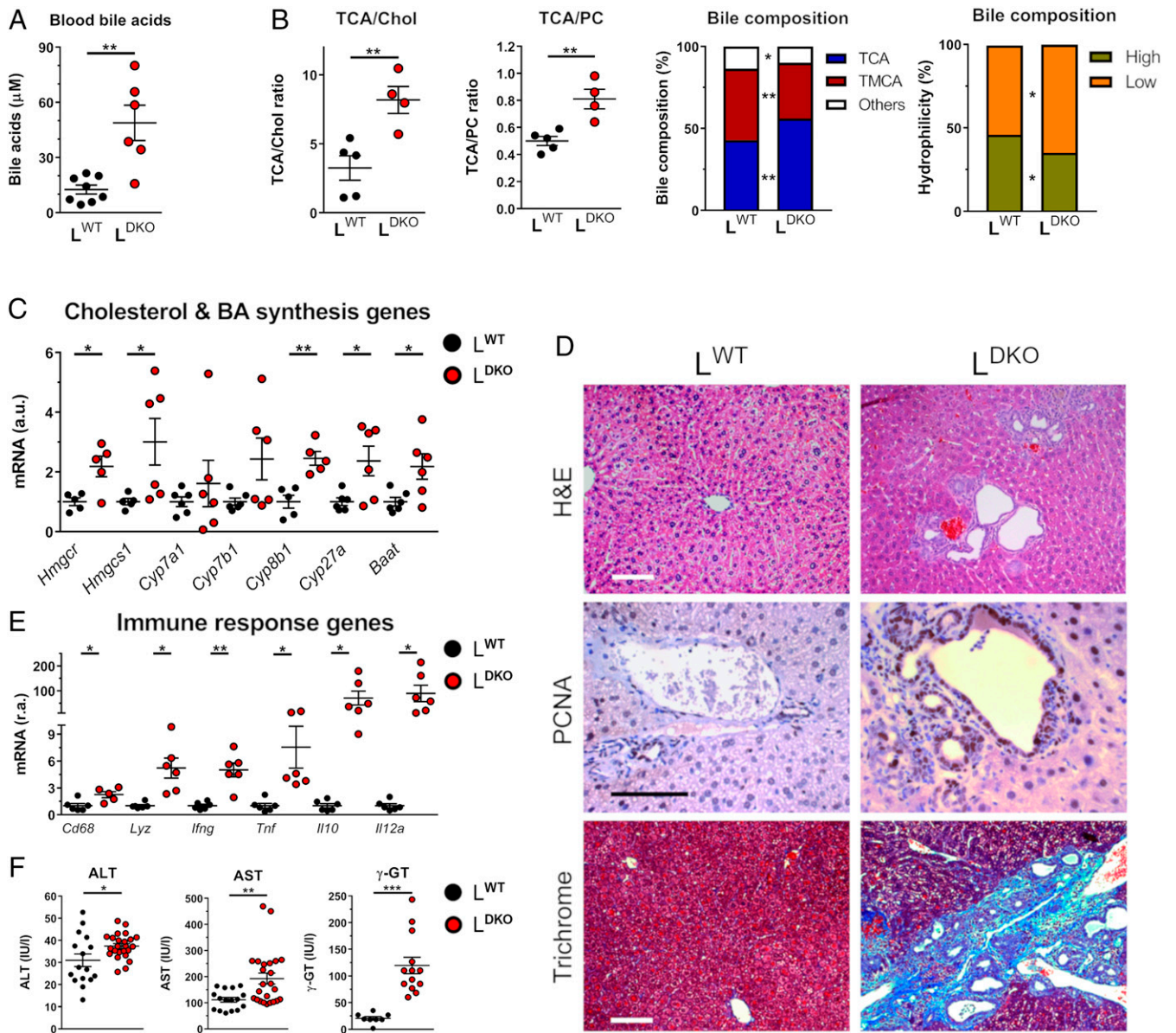


Fig. 1. Hepatic JNK deficiency alters bile acid production and causes cholestasis. (A) L^{WT} and L^{DKO} mice (age 6 mo) were fasted overnight, and blood was collected for measuring bile acids (mean \pm SEM; $n = 6-11$). Student's t test differences between L^{DKO} and L^{WT} are indicated (** $P < 0.01$). (B) The composition of bile fluid collected from the gall bladder was examined by measurement of the ratio of BAs to cholesterol (Chol) or PC and the different type of BA. TCA, taurocholic acid; TMCA, tauromuricholic acids. The data presented are the mean \pm SEM ($n = 4-5$). Student's t test differences between L^{DKO} and L^{WT} are indicated (* $P < 0.05$; ** $P < 0.01$). (C) L^{DKO} and L^{WT} mice (age 6 mo) were fasted overnight prior to removal of the liver. The expression of genes related to cholesterol synthesis (*Hmgcr* and *Hmgcs1*) and BA synthesis (*Cyp7a1*, *Cyp7b1*, *Cyp27a1*, *Baat*, *Cyp27a*, *Cyp8b1*) was measured by quantitative RT-PCR (mean \pm SEM; $n = 5-6$) and normalized to the amount of *18S* RNA in each sample. Student's t test differences between L^{DKO} and L^{WT} are indicated (* $P < 0.05$; ** $P < 0.01$). (D) Representative liver sections prepared from mice (age 10 mo) stained with hematoxylin and eosin (H&E), an antibody to PCNA, and Masson Trichrome (Trichrome) are presented. (Scale bar, 100 μ m.) (E) The expression of genes related to inflammation was evaluated by RT-PCR. (mean \pm SEM; $n = 5-6$) and normalized to the amount of *18S* RNA in each sample. Student's t test differences between L^{DKO} and L^{WT} are indicated (* $P < 0.05$). (F) Liver damage assessed from serum measurements of ALT, AST, and γ -GT. (mean \pm SEM; $n = 11-24$). Student's t test differences between L^{DKO} and L^{WT} are indicated (* $P < 0.05$; ** $P < 0.01$, *** $P < 0.001$).

in which defects in BA homeostasis are linked to cholangiocarcinoma (Fig. 6).

Previous studies have established that hepatic JNK deficiency can suppress cholangiocyte proliferation and oncogenic transformation in a p53/Kras-induced model of cholangiosarcoma (35) and promotes cholangiocarcinoma in deethylnitrosamine and NEMO deficiency models of liver cancer (36). The results of the present study demonstrate that hepatic JNK deficiency is sufficient for the development of cholangiocyte malignancy (Fig. 2).

PPAR α is an important modulator of liver metabolism controlling lipid and BA homeostasis, and its activation has been shown to decrease fatty liver disease (19, 37, 38). We report that JNK-mediated repression of PPAR α causes changes in BA homeostasis which suppress cholangiocyte proliferation. Consequently, JNK deficiency stimulates cholangiocyte proliferation and promotes the development of cholangiocarcinoma. This increased proliferation is mediated by the altered BA metabolism and the elevated hepatic expression of FXR/FGF15/FGFR4 that

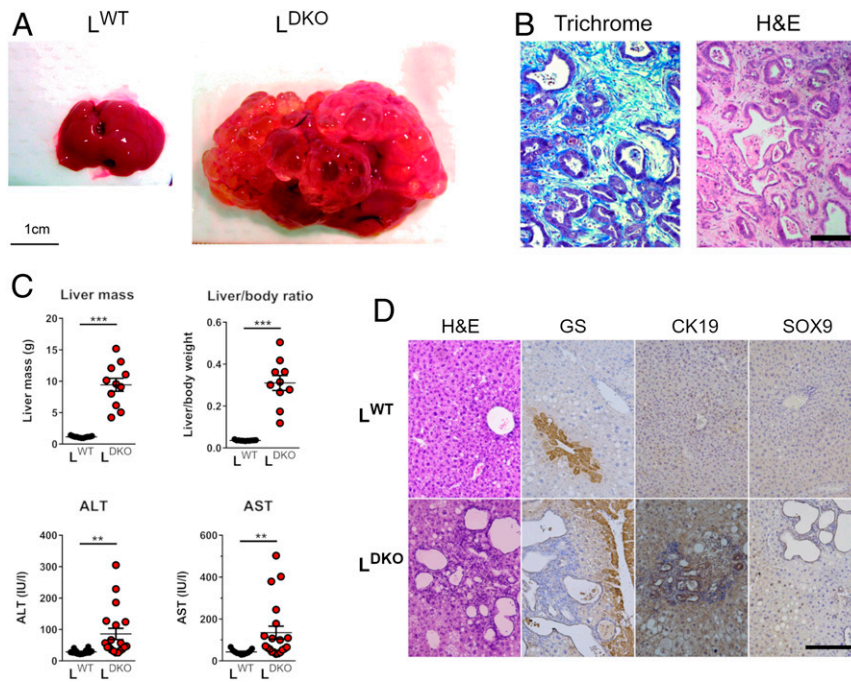


Fig. 2. Hepatic JNK deficiency progress to cholangiocarcinoma. (A) Representative livers of L^{WT} and L^{DKO} mice at age 14 mo are shown. (B) Representative sections of the liver of chow-fed L^{DKO} mice stained with H&E and Masson Trichrome (Trichrome). (Scale bar, 100 μm .) (C) The liver mass and liver damage measured by levels of ALT and AST (mean \pm SEM; $n = 11\text{--}20$) are presented. Student's t test differences between L^{DKO} and L^{WT} are indicated (** $P < 0.01$, *** $P < 0.001$). (D) Representative liver sections of 10-mo-old L^{DKO} and L^{WT} mice stained with GS, Cytokeratin 19 (CK19), and Sox9. (Scale bar, 100 μm .)

triggers ERK activation in cholangiocytes (Fig. 6). Our results have strong translational implications for obesity treatment. Activation of FXR by BA triggers the secretion of FGF15/FGF19 in humans (39), and the beneficial effects of FGF expression on the obese metabolic profile has been well characterized (40). However, the clinical use of FGF has been debated due to the potential for increasing liver tumor development (41, 42).

Hepatic PPAR α is an important mediator of this regulatory cascade. Indeed, PPAR α deficiency dramatically suppresses the phenotypes caused by JNK deficiency. Nevertheless, the role of PPAR α in liver cancer remains unclear. While some studies have demonstrated that PPAR α activation might promote liver cancer (43–45), others indicate that PPAR α activation may be neutral or suppress liver cancer development (46–49). This could be due to different experimental conditions used in these studies. In our

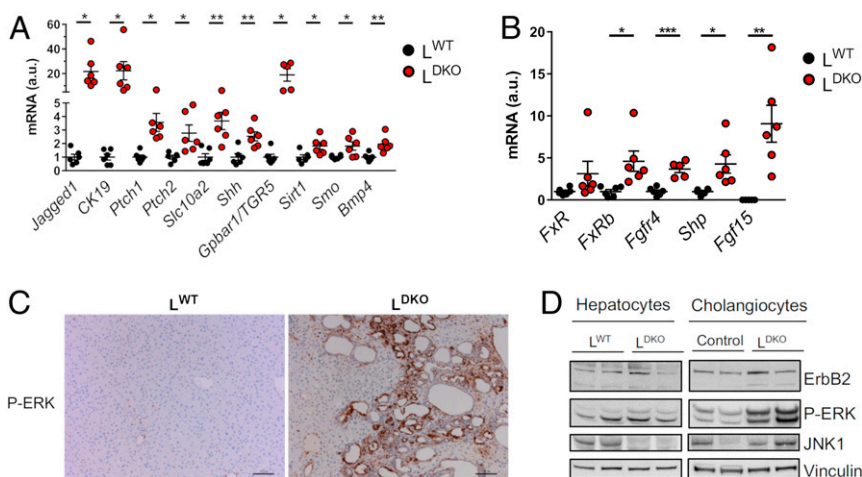


Fig. 3. ERK pathway activation accompanies the development of cholangiocarcinoma induced by hepatic JNK deficiency. (A) The expression of genes related to cholangiocytes proliferation was evaluated by RT-PCR in 14-mo-old L^{WT} and L^{DKO} mice and normalized to the amount of *18S* RNA in each sample (mean \pm SEM; $n = 5\text{--}6$). Student's t test differences between L^{DKO} and L^{WT} are indicated (* $P < 0.05$; ** $P < 0.01$). (B) The expression of genes related to the nuclear factor FXR (*Fxr*, *Fxr*b, *Shp*, *Fgfr*4) and *Fgf*15 was measured by quantitative RT-PCR in L^{WT} and L^{DKO} liver from mice at age 6 mo (mean \pm SEM; $n = 5\text{--}6$) normalized to the amount of *Actb* mRNA in each sample. Student's t tests between L^{DKO} and L^{WT} are indicated (* $P < 0.05$; ** $P < 0.01$, *** $P < 0.001$). (C) Representative liver sections of L^{DKO} and L^{WT} mice (age 10 mo) stained with phospho-ERK. (Scale bar, 100 μm .) (D) Comparative protein expression of ErbB2, phospho-ERK, and JNK1 in hepatocytes and cholangiocytes in L^{WT} and L^{DKO} mice was evaluated by immunoblot analysis. Vinculin was used as a loading control.

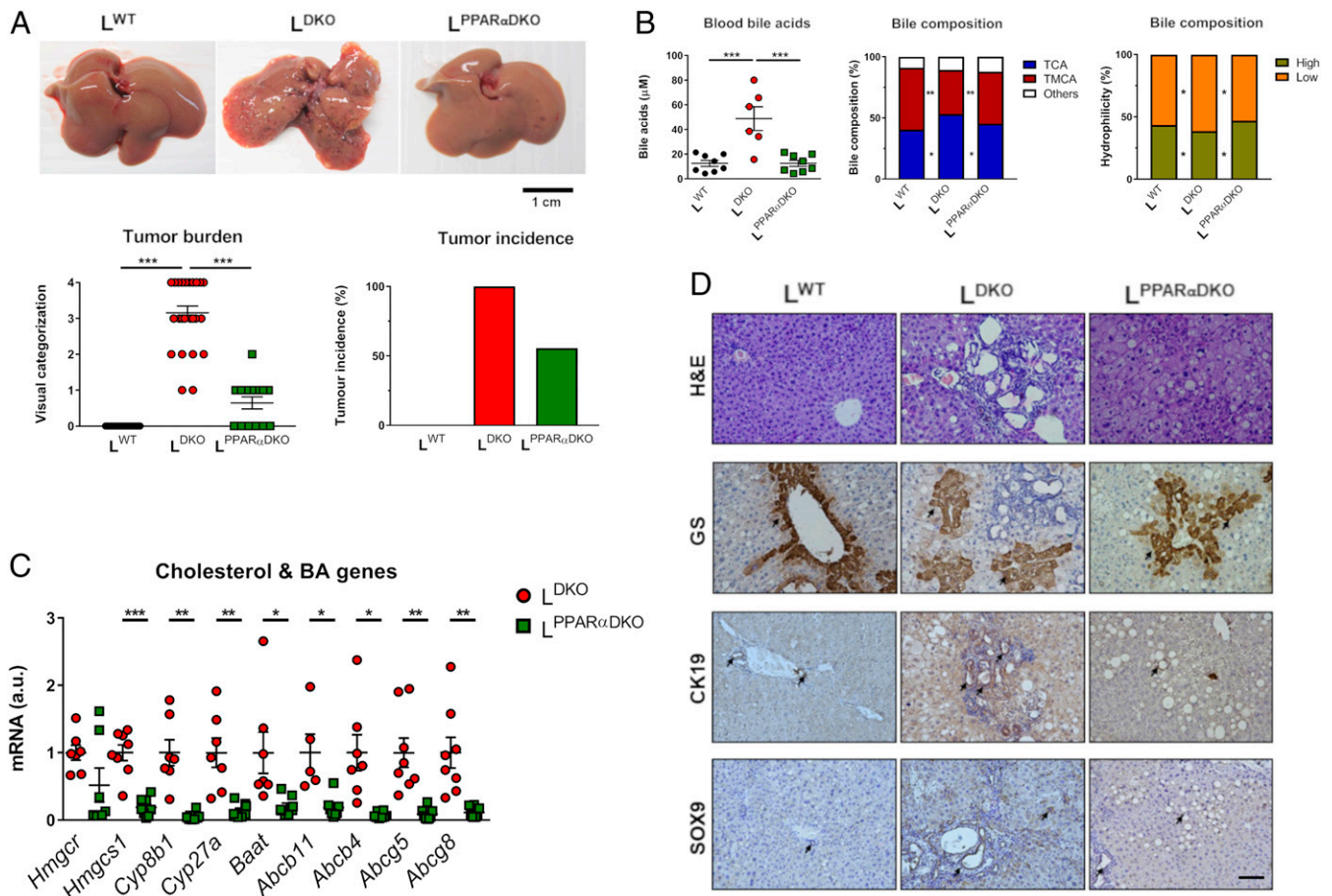


Fig. 4. PPAR α deficiency reduces liver cancer induced by hepatic JNK deficiency. (A) Representative livers, tumor burden, and incidence in 11-mo-old L^{WT}, L^{DKO}, and L^{PPAR α DKO} mice (mean \pm SEM; $n = 14 \sim 25$). (B) The amount of bile acid in the blood was measured (mean \pm SE; $n = 7\text{--}11$). The composition of bile fluid collected from the gall bladder was examined. Two-way ANOVA differences between L^{PPAR α DKO}, L^{DKO}, and L^{WT} are indicated (* $P < 0.05$; ** $P < 0.01$). (C) The expression of genes related to cholesterol synthesis (*Hmgcr* and *Hmgcs1*), BA synthesis, and transporters (*Cyp27a1*, *Baat*, *Cyp27a*, *Cyp8b1*, *Abcb11*, *Abcb4*, *Abcg5*, *Abcg8*) was measured by quantitative RT-PCR (mean \pm SEM; $n = 5\text{--}8$) normalized to the amount of *Actb* mRNA in each sample. Two-way ANOVA differences between L^{DKO} and L^{PPAR α DKO} are indicated (* $P < 0.05$; ** $P < 0.01$, *** $P < 0.001$). (D) Representative liver sections of 10-mo-old L^{WT}, L^{DKO}, and L^{PPAR α DKO} mice stained with GS, Cytokeratin 19 (CK19), and Sox9. (Scale bar, 100 μm .)

system, the protumorigenic effect of PPAR α activation is due, in part, to an alteration in BA metabolism that drives ERK activation, suggesting that PPAR α activation is a critical factor in cholangiocarcinoma development and progression.

The role of JNK/PPAR α /FGF signaling in lipid metabolism suggests that this pathway could represent a target for the treatment for steatosis and obesity. However, the possible contribution of this pathway to carcinogenic progression represents a serious problem for long-term treatment. Our analysis suggests that treatment strategies using long-term JNK inhibition should consider the potential risk of cholangiocarcinoma development among the possible secondary effects of this treatment.

Methods

Animals. PPAR α knockout mice (B6;12954-Ppara^{tm1Gonz/J}; RRID:IMSR_JAX:008154) and Albumin-Cre mice (B6.Cg-Speer6-ps1^{Tg(Alb-cre)21Mng/J}; RRID:IMSR_JAX:003574) were purchased from the Jackson Laboratory and backcrossed for 10 generations to the C57BL/6J background (Jackson Laboratory; RRID:IMSR_JAX:000664). Mice with compound JNK1/2 deficiency in hepatocytes (L^{DKO}) have been described (50, 51). Genotypes were identified by PCR analysis of genomic DNA isolated from mouse tails. All experiments were performed using male mice. Mice were housed in a pathogen-free animal facility and kept on a 12-h light/dark cycle at constant temperature and humidity.

All animal experiments conformed to European Union (EU) Directive 2010/63EU and Recommendation 2007/526/EC, enforced in Spanish law under Real

Decreto 53/2013 and the Institutional Animal Care and Use Committee of the University of Massachusetts Medical School.

Serum Analysis. Plasma transaminase activity was assessed with the ALT and AST Reagent Kit (Biosystems Reagents) using a Benchmark Plus microplate spectrophotometer (Bio-Rad). Plasma concentration of nonsulfated bile acids was measured with the Bile Acid Assay Kit (Sigma-Aldrich) using a Fluoroskan Ascent fluorescence multiwell plate reader (Thermo Labsystems).

Table 1. PPAR α deficiency reduces carcinogenesis markers in JNK1/2-deficient livers

	L ^{WT}	L ^{DKO}	L ^{PPARαDKO}
Anisokaryosis	–	++	+
Apoptosis	–	+++	+
Necrotic foci	–	+++	++
Cellular hypertrophy	–	+++	++
Ductogenesis	–	+++	+
Cystogenesis	–	+++	++
Microsteatosis	+	+	+++
Macrosteatosis	–	++	+++
Lymphocytic inflammation	–	+++	+
Dysplasia	–	+++	+
Mitosis	+	+++	+

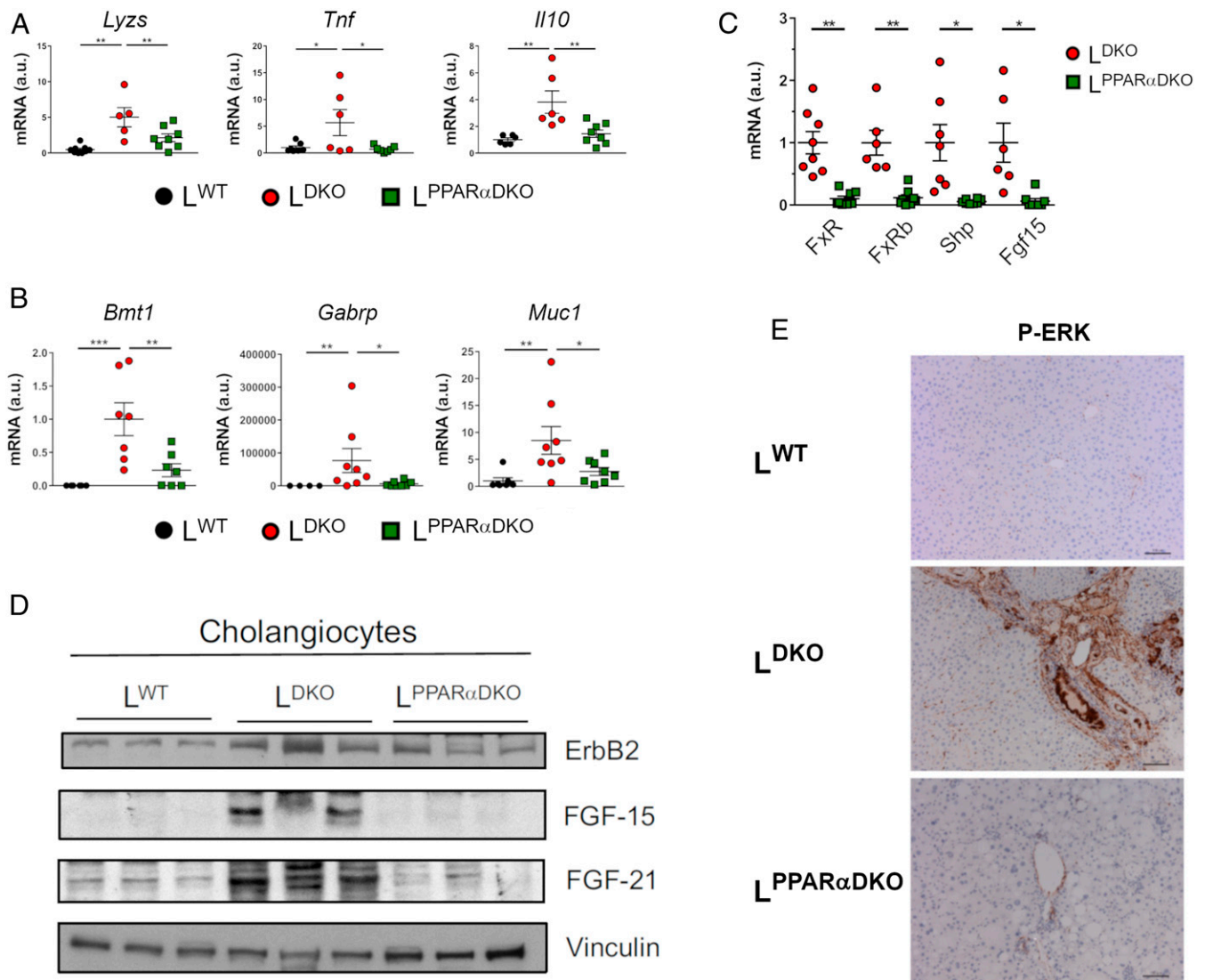


Fig. 5. PPAR α deficiency reduces liver cholangiocarcinoma induced by hepatic JNK deficiency. (A and B) The expression of genes related to inflammation and cholangiocarcinoma was evaluated by quantitative RT-PCR (mean \pm SEM; $n = 4-8$) normalizing to the amount of *Actb* mRNA in each sample. Two-way ANOVA differences between L^{DKO} and L^{PPAR α DKO} are indicated (* $P < 0.05$; ** $P < 0.01$, *** $P < 0.001$). (C) The expression of genes related to nuclear factor FXR pathway (*Fxr*, *FxrB*, *Shp*, *Fgf4*, and *Fgf15*) was evaluated in L^{DKO} and L^{PPAR α DKO} livers by quantitative RT-PCR (mean \pm SEM; $n = 6-8$) normalizing to the amount of *Actb* mRNA in each sample. Student's *t* test differences between L^{DKO} and L^{PPAR α DKO} are indicated (* $P < 0.05$; ** $P < 0.01$). (D) Representative Western blots of ErbB2, FGF15, and FGF21 in cholangiocytes in L^{DKO}, L^{PPAR α DKO}, and L^{WT} mice ($n = 3$). Vinculin was used as a loading control. (E) Representative sections of the liver of 10-mo-old L^{DKO}, L^{PPAR α DKO}, and L^{WT} mice stained with Phospho-ERK. (Scale bar, 100 μ m.)

Histochemistry. Histology was performed using tissue fixed in 10% formalin for 24 h, dehydrated, and embedded in paraffin. Sections (7 μ m) were cut and stained using hematoxylin and eosin (American Master Tech Scientific). Sections were also incubated with Bouin's fluid overnight, counterstain with hematoxylin (Sigma), and then stained with Masson-Trichrome stain (American Master Tech Scientific). Immunohistochemistry was performed by staining tissue sections with antibodies against PCNA (biotinylated from ThermoFisher MS-106-B; RRID:AB_64272), SOX9 (Abcam ab3697; RRID:AB_304012), glutamine synthetase (Abcam ab73593; RRID:AB_2247588), cytokeratin 19 (Abcam ab15463; RRID:AB_2281021), or phospho-p44/42 MAPK (Thr202/Tyr204) (Cell Signaling Technology #9101). Streptavidin-conjugated horseradish peroxidase (Biogenex) and the substrate 3,3'-diaminobenzidine (Vector Laboratories) were used followed by brief counterstaining with Mayer's hematoxylin (Sigma).

Analysis of Biliary Lipids. Bile was collected from the gall bladder following cholecystectomy. We determined cholesterol and phospholipids using an enzymatic assay (Wako). Total bile acids were measured using Hall's Bile Stain Kit (American MasterTech). Bile acid species were examined by a modification of the method described by ref. 52 using an HPLC-MS/MS (6410 Triple

Quad LC/MS, Agilent Technologies). Chromatographic separation was achieved with gradient elution using a Zorbax Eclipse XDB-C18 column (150 \times 4.6 mm, 5 μ m) kept at 35 $^{\circ}$ C and a flow rate of 500 μ L/min. Initial mobile phase was 80:20 methanol/water, both containing 5 mM ammonium acetate and 0.01% formic acid, pH 4.6, and it was changed to 97:3 methanol/water over 9 min and then returned to 80:20 in 1 min. Electrospray ionization in negative mode was used, with the following conditions: gas temperature 350 $^{\circ}$ C, gas flow 8 L/min, nebulizer 10 psi, capillary voltage 2,500 V. MS/MS acquisition was performed in multiple reaction monitoring mode using the specific *m/z* transitions: [M-H]⁻ ion to 80.2 for taurine-conjugated bile acids and [M-H]⁻ ion to 74 for glycine-conjugated bile acids. Free bile acids did not generate characteristic ion fragments, as reported by others (52), and transition from unfragmented precursor molecular ions 407.1–407.1, 391.3–391.3, and 375.3–375.3 were selected for trihydroxylated, dehydroxylated, and monohydroxylated free bile acids, respectively.

Isolation of Hepatocytes and Cholangiocytes. Mice livers were perfused using a peristaltic pump with 40 mL of Hanks Balanced Salt Solution (with 10 mM Hepes [pH 7.4] and 1 mM EGTA; without MgCl₂ and CaCl₂) and then with

1 mg/mL of collagenase type I (Worthington). Hepatocytes were collected as a cell suspension in Dulbecco's Modified Eagle's Medium/F12 Medium (10% FBS, 0.2 mg/mL BSA, 5% sodium pyruvate, 10 mM Hepes [pH 7.4], 1% L-glutamine, 1% Penicillin/Streptomycin, 0.51 mg/mL NaHCO₃). Biliary trees were collected in Williams' medium supplemented with 5 mM Hepes (pH 7.4) and 1 mg/mL collagenase type I prior to incubation (1 h) at 37 °C to isolate cholangiocytes. The cells were washed with PBS before protein extraction as previously described (53).

Western Blot Analysis. Hepatocytes and cholangiocytes proteins were extracted in lysis buffer (50 mM Tris-HCl pH 7.5, 1 mM EGTA, 1 mM EDTA pH 8.0, 50 mM sodium fluoride, 1 mM sodium β-glycerophosphate, 5 mM sodium pyrophosphate, 1 mM sodium orthovanadate, 0.27 M sucrose, 1% Triton X-100, 0.1 mM PMSF, 0.1% 2-mercaptoethanol, 1 μg/mL leupeptin, and 1 μg/mL aprotinin). Extracts were separated by SDS-PAGE and transferred to 0.2-μm pore-size nitrocellulose membranes (Bio-Rad). Blots were probed with primary antibodies to ErbB2 (Cat# ab16901, Abcam; RRID: [AB_443537](#)), phospho-ERK (Cat#9101, Cell Signaling Biotechnology; RRID: [AB_330744](#)), JNK1 (Cat# sc-1648, Santa Cruz Biotechnology; RRID: [vAB_675868](#)), FGF-15 (Cat# sc-514647, Santa Cruz Biotechnology), FGF-21 (Cat# RD281108100, BioVendor Laboratory Medicine; RRID: [AB_2034054](#)), and Vinculin (Cat#V4505, Sigma; RRID: [AB_477617](#)). All antibodies were used at 1:1,000 dilution. The membranes were washed and incubated with an appropriate horseradish peroxidase-conjugated secondary antibody (GE Healthcare), and immune complexes were detected using an enhanced chemiluminescent substrate (Clarity Western ECL substrate; Bio-Rad).

RNA-seq Analysis. Liver RNA-seq data from chow-fed L^{WT} and L^{DKO} (GEO GSE55190) were examined (7). Sequencing reads were preprocessed by means of a pipeline that used FastQC, to assess read quality, and Cutadapt to trim sequencing reads, eliminating Illumina adaptor remains, and to discard reads that were shorter than 30 bp. Resulting reads were mapped against reference transcriptome GRCm38.91 and quantified using RSEM. Percentages of reads participating in at least one reported alignment were around 80%. Expected expression counts calculated with RSEM were then processed with an analysis pipeline that used the Bioconductor package Limma for normalization (using TMM method) and differential expression testing, taking only into account those genes expressed with at least 1 count per million in a number of samples equal to the number of replicate samples of

the condition with less replicates. Significant expression changes between wild type (WT) and JNK1/2 double-KO conditions, with Benjamini and Hochberg adjusted *P* value < 0.05, were detected for 44 genes. Given that the collection of differentially expressed genes was relatively small, an adjusted *P* value threshold of 0.2 was applied for further analyses. The resulting collection of 739 genes was then used for functional enrichment analyses with IPA (Ingenuity Pathway Analysis), to discover overrepresented gene lists derived from Ingenuity's proprietary knowledge-base (IPAKB). IPAKB-derived gene lists consisted of collections of genes belonging to the same signaling or metabolic pathway (Canonical Pathway analyses), or regulated by the same molecule (Upstream Regulator analyses). In general, enrichments associated to Benjamini-Hochberg adjusted *P* value < 0.05 are considered significant. Importantly, IPA may issue predictions on the activation state of pathways or regulators in the form of a parameter called *z* score; activation or inhibition is indicated by positive or negative values, respectively. Other data manipulations and graphical representations (heatmaps, bar plots, and scatter plots) were produced with statistical package R.

Real-Time qPCR. Total RNA was isolated from liver and tumor tissue using the RNeasy Mini Kit (Qiagen) with on-column DNase I-digestion. cDNA (complementary DNA) was synthesized with the High-Capacity cDNA Reverse Transcription Kit (Applied Biosystems). Taqman[®] assays were performed using the probes listed in *SI Appendix, Table S1* (Applied Biosystems). Sequences of primers used for quantitative real-time PCR (RT-PCR) are provided in *SI Appendix, Table S2*. Expression levels were normalized to 18S using Taqman[®] assays (430449011032, Applied Biosystems) (Figs. 1 and 3A and *SI Appendix, Fig. S1*) or *Actb* (Figs. 3B, 4, and 5) mRNA. qRT-PCR was performed using the Fast SYBR Green system (Applied Biosystems) in a 7900HT Fast Real-Time PCR thermal cycler (Applied Biosystems). A dissociation curve program was employed after each reaction to verify purity of the PCR products. The expression of mRNA was examined by quantitative PCR analysis using a 7500 Fast Real-Time PCR machine.

Statistics. Differences between groups were examined for statistical significance using two-tailed unpaired Student's *t* test (with Welch's correction when variances were different) or ANOVA coupled to Bonferroni's post-test. Kaplan-Meier analysis was performed using the log-rank test. Statistical details and experimental *n* are specified in figure legends.

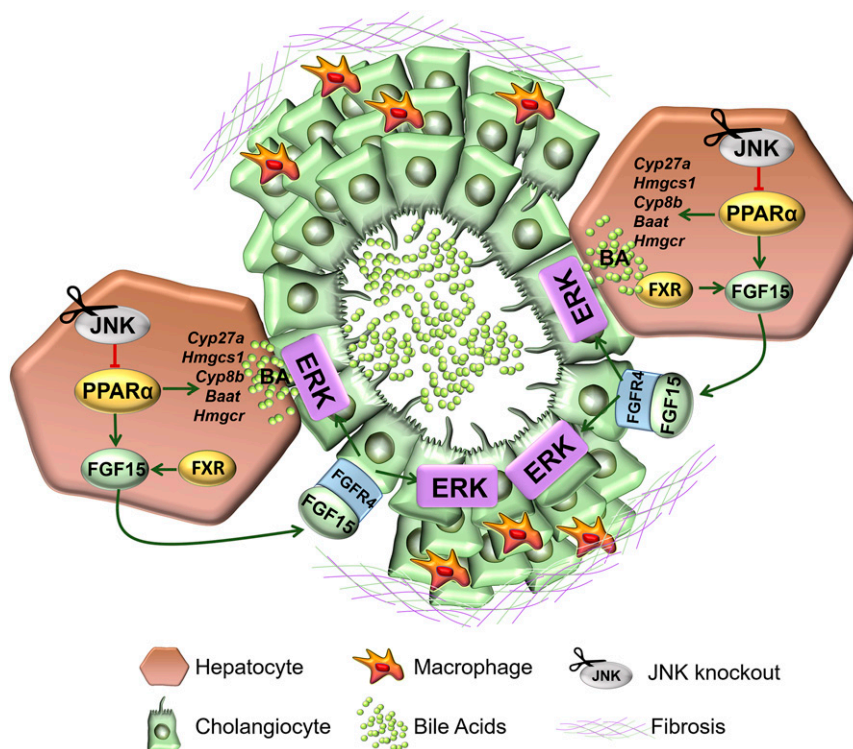


Fig. 6. Schematic illustration of JNK-regulated cholangiocarcinoma development in the liver.

Statistical analyses were performed with the GraphPad Prism 7 software (RRID:SCR_002798).

Material and Data Availability. Sources for materials used in this study are described in Methods. The raw data obtained for this study are presented in *SI Appendix, Fig. 3D* and *Dataset S1*.

ACKNOWLEDGMENTS. We thank S. Bartlett for English editing and David Garlick (University of Massachusetts Medical School) for pathological examination of tissue sections. We are grateful to the CNIC Advanced Imaging and Animal facility for technical support. G.S. (RYC-2009-04972) and F.J.C. (RYC-2014-15242) are investigators of the Ramón y Cajal Program. E.M. was awarded a La Caixa fellowship. C.F. was awarded a Sara Borrell contract (CD19/00078). This work was funded by grants supported in part by funds

from the European Regional Development Fund: EU's Seventh Framework Programme (FP7/2007-2013) ERC 260464, EFS/Lilly European Diabetes Research Programme Dr. Sabio, 2017 Leonardo Grant for Researchers and Cultural Creators, BBVA Foundation (Investigadores-BBVA-2017) IN[17], BBM_BAS_0066, MINECO-FEDER SAF2016-79126-R, and Comunidad de Madrid IMMUNOTHER-CAN-CM S2010/BMD-2326 and B2017/BMD-3733 and La Asociación Española contra el Cáncer (to G.S.); EXOHEP-CM S2017/BMD-3727 and the European Cooperation in Science & Technology (COST) Action CA17112 (to F.J.C.); MINECO Retos SAF2016-78711, the AMMF Cholangiocarcinoma Charity 2018/117, Nano-Liver-CM Y2018/NMT-4949, UCM-25-2019, ERAB EA/18-14 (to F.J.C.). F.J.C. is a Gilead Liver Research Scholar. Grant DK R01 DK107220 from the NIH (to R.J.D.); and PI16/00598 from Carlos III Institute of Health, Spain (to J.J.G.M.). The CNIC is supported by the Ministerio de Ciencia, Innovación y Universidades, and the Pro-CNIC Foundation and is a Severo Ochoa Center of Excellence (SEV-2015-0505).

1. D. M. Parkin, F. Bray, J. Ferlay, P. Pisani, Global cancer statistics, 2002. *CA Cancer J. Clin.* **55**, 74–108 (2005).
2. H. B. El-Serag, J. A. Davila, N. J. Petersen, K. A. McGlynn, The continuing increase in the incidence of hepatocellular carcinoma in the United States: An update. *Ann. Intern. Med.* **139**, 817–823 (2003).
3. S. A. Khan, S. Tavolari, G. Brandi, Cholangiocarcinoma: Epidemiology and risk factors. *Liver Int.* **39** (suppl. 1), 19–31 (2019).
4. S. A. Khan et al., British Society of Gastroenterology, Guidelines for the diagnosis and treatment of cholangiocarcinoma: An update. *Gut* **61**, 1657–1669 (2012).
5. E. Manieri, G. Sabio, Stress kinases in the modulation of metabolism and energy balance. *J. Mol. Endocrinol.* **55**, R11–R22 (2015).
6. G. Sabio, R. J. Davis, cJun NH2-terminal kinase 1 (JNK1): Roles in metabolic regulation of insulin resistance. *Trends Biochem. Sci.* **35**, 490–496 (2010).
7. S. Vernia et al., The PPAR α -FGF21 hormone axis contributes to metabolic regulation by the hepatic JNK signaling pathway. *Cell Metab.* **20**, 512–525 (2014).
8. S. Vernia, J. Cavanagh-Kyros, T. Barrett, C. Tournier, R. J. Davis, Fibroblast growth factor 21 mediates glycemic regulation by hepatic JNK. *Cell Rep.* **14**, 2273–2280 (2016).
9. T. Gulick, S. Cresci, T. Caira, D. D. Moore, D. P. Kelly, The peroxisome proliferator-activated receptor regulates mitochondrial fatty acid oxidative enzyme gene expression. *Proc. Natl. Acad. Sci. U.S.A.* **91**, 11012–11016 (1994).
10. R. H. Unger, Y. T. Zhou, Lipotoxicity of beta-cells in obesity and in other causes of fatty acid spillover. *Diabetes* **50** (suppl. 1), S118–S121 (2001).
11. R. M. Evans, G. D. Barish, Y. X. Wang, PPARs and the complex journey to obesity. *Nat. Med.* **10**, 355–361 (2004).
12. R. A. Memon et al., Up-regulation of peroxisome proliferator-activated receptors (PPAR-alpha) and PPAR-gamma messenger ribonucleic acid expression in the liver in murine obesity: Troglitazone induces expression of PPAR-gamma-responsive adipose tissue-specific genes in the liver of obese diabetic mice. *Endocrinology* **141**, 4021–4031 (2000).
13. E. Ip et al., Central role of PPARalpha-dependent hepatic lipid turnover in dietary steatohepatitis in mice. *Hepatology* **38**, 123–132 (2003).
14. N. C. Teoh et al., Short-term therapy with peroxisome proliferation-activator receptor-alpha agonist Wy-14,643 protects murine fatty liver against ischemia-reperfusion injury. *Hepatology* **51**, 996–1006 (2010).
15. P. R. Holden, J. D. Tugwood, Peroxisome proliferator-activated receptor alpha: Role in rodent liver cancer and species differences. *J. Mol. Endocrinol.* **22**, 1–8 (1999).
16. D. Panigrahy et al., PPARalpha agonist fenofibrate suppresses tumor growth through direct and indirect angiogenesis inhibition. *Proc. Natl. Acad. Sci. U.S.A.* **105**, 985–990 (2008).
17. M. Maggiora, M. Oraldi, G. Muzio, R. A. Canuto, Involvement of PPAR α and PPAR γ in apoptosis and proliferation of human hepatocarcinoma HepG2 cells. *Cell Biochem. Funct.* **28**, 571–577 (2010).
18. D. Yamasaki et al., Fenofibrate suppresses growth of the human hepatocellular carcinoma cell via PPAR α -independent mechanisms. *Eur. J. Cell Biol.* **90**, 657–664 (2011).
19. T. Li, J. Y. Chiang, Regulation of bile acid and cholesterol metabolism by PPARs. *PPAR Res.* **2009**, 501739 (2009).
20. C. Yoo et al., Multiplexed gene expression profiling identifies the FGFR4 pathway as a novel biomarker in intrahepatic cholangiocarcinoma. *Oncotarget* **8**, 38592–38601 (2017).
21. S. Miura et al., Fibroblast growth factor 19 expression correlates with tumor progression and poorer prognosis of hepatocellular carcinoma. *BMC Cancer* **12**, 56 (2012).
22. H. Shapiro, A. A. Kolodziejczyk, D. Halstuch, E. Elinav, Bile acids in glucose metabolism in health and disease. *J. Exp. Med.* **215**, 383–396 (2018).
23. P. C. de Groen, G. J. Gores, N. F. LaRusso, L. L. Gunderson, D. M. Nagorney, Biliary tract cancers. *N. Engl. J. Med.* **341**, 1368–1378 (1999).
24. V. Keitel et al., The G-protein coupled bile salt receptor TGR5 is expressed in liver sinusoidal endothelial cells. *Hepatology* **45**, 695–704 (2007).
25. P. A. Dawson, T. Lan, A. Rao, Bile acid transporters. *J. Lipid Res.* **50**, 2340–2357 (2009).
26. D. A. Piccoli, N. B. Spinner, Alagille syndrome and the Jagged1 gene. *Semin. Liver Dis.* **21**, 525–534 (2001).
27. J. Fan et al., Bone morphogenetic protein 4 mediates bile duct ligation induced liver fibrosis through activation of Smad1 and ERK1/2 in rat hepatic stellate cells. *J. Cell. Physiol.* **207**, 499–505 (2006).
28. M. Yanai et al., FGF signaling segregates biliary cell-lineage from chick hepatoblasts cooperatively with BMP4 and ECM components in vitro. *Dev. Dyn.* **237**, 1268–1283 (2008).
29. L. Yang et al., A single-cell transcriptomic analysis reveals precise pathways and regulatory mechanisms underlying hepatoblast differentiation. *Hepatology* **66**, 1387–1401 (2017).
30. T. Li, J. Y. Chiang, Bile acids as metabolic regulators. *Curr. Opin. Gastroenterol.* **31**, 159–165 (2015).
31. P. L. Jansen et al., The ascending pathophysiology of cholestatic liver disease. *Hepatology* **65**, 722–738 (2017).
32. K. Allen, H. Jaeschke, B. L. Copple, Bile acids induce inflammatory genes in hepatocytes: A novel mechanism of inflammation during obstructive cholestasis. *Am. J. Pathol.* **178**, 175–186 (2011).
33. W. Zhang et al., A weighted relative difference accumulation algorithm for dynamic metabolomics data: Long-term elevated bile acids are risk factors for hepatocellular carcinoma. *Sci. Rep.* **5**, 8984 (2015).
34. S. Sombaththeera et al., Total serum bile acid as a potential marker for the diagnosis of cholangiocarcinoma without jaundice. *Asian Pac. J. Cancer Prev.* **16**, 1367–1370 (2015).
35. D. Yuan et al., Kupffer cell-derived Tnf triggers cholangiocellular tumorigenesis through JNK due to chronic mitochondrial dysfunction and ROS. *Cancer Cell* **31**, 771–789.e6 (2017).
36. F. J. Cubero et al., Loss of c-Jun N-terminal kinase 1 and 2 function in liver epithelial cells triggers biliary hyperproliferation resembling cholangiocarcinoma. *Hepatology* **62**, 834–851 (2015).
37. M. A. Abdelmegeed et al., PPARalpha expression protects male mice from high fat-induced nonalcoholic fatty liver. *J. Nutr.* **141**, 603–610 (2011).
38. J. E. Yeon et al., Reduced expression of peroxisome proliferator-activated receptor-alpha may have an important role in the development of non-alcoholic fatty liver disease. *J. Gastroenterol. Hepatol.* **19**, 799–804 (2004).
39. T. Inagaki et al., Fibroblast growth factor 15 functions as an enterohepatic signal to regulate bile acid homeostasis. *Cell Metab.* **2**, 217–225 (2005).
40. V. J. Nies et al., Fibroblast growth factor signaling in metabolic regulation. *Front. Endocrinol. (Lausanne)* **6**, 193 (2016).
41. M. Zhou et al., Mouse species-specific control of hepatocarcinogenesis and metabolism by FGF19/FGF15. *J. Hepatol.* **66**, 1182–1192 (2017).
42. G. Cui et al., Up-regulation of FGF15/19 signaling promotes hepatocellular carcinoma in the background of fatty liver. *J. Exp. Clin. Cancer Res.* **37**, 136 (2018).
43. J. M. Peters, R. C. Cattley, F. J. Gonzalez, Role of PPAR alpha in the mechanism of action of the nongenotoxic carcinogen and peroxisome proliferator Wy-14,643. *Carcinogenesis* **18**, 2029–2033 (1997).
44. T. Hays et al., Role of peroxisome proliferator-activated receptor-alpha (PPARalpha) in bezafibrate-induced hepatocarcinogenesis and cholestasis. *Carcinogenesis* **26**, 219–227 (2005).
45. J. Nishimura et al., Effect of fenofibrate on oxidative DNA damage and on gene expression related to cell proliferation and apoptosis in rats. *Toxicol. Sci.* **97**, 44–54 (2007).
46. K. Takashima, Y. Ito, F. J. Gonzalez, T. Nakajima, Different mechanisms of DEHP-induced hepatocellular adenoma tumorigenesis in wild-type and Ppar alpha-null mice. *J. Occup. Health* **50**, 169–180 (2008).
47. F. Heindryckx, I. Colle, H. Van Vlierbergh, Experimental mouse models for hepatocellular carcinoma research. *Int. J. Exp. Pathol.* **90**, 367–386 (2009).
48. C. Cheung et al., Diminished hepatocellular proliferation in mice humanized for the nuclear receptor peroxisome proliferator-activated receptor alpha. *Cancer Res.* **64**, 3849–3854 (2004).
49. K. Morimura, C. Cheung, J. M. Ward, J. K. Reddy, F. J. Gonzalez, Differential susceptibility of mice humanized for peroxisome proliferator-activated receptor alpha to Wy-14,643-induced liver tumorigenesis. *Carcinogenesis* **27**, 1074–1080 (2006).
50. M. Das, D. S. Garlick, D. L. Greiner, R. J. Davis, The role of JNK in the development of hepatocellular carcinoma. *Genes Dev.* **25**, 634–645 (2011).
51. M. Das et al., Induction of hepatitis by JNK-mediated expression of TNF-alpha. *Cell* **136**, 249–260 (2009).
52. L. Ye, S. Liu, M. Wang, Y. Shao, M. Ding, High-performance liquid chromatography-tandem mass spectrometry for the analysis of bile acid profiles in serum of women with intrahepatic cholestasis of pregnancy. *J. Chromatogr. B Analyt. Technol. Biomed. Life Sci.* **860**, 10–17 (2007).
53. L. Barbier-Torres et al., Histone deacetylase 4 promotes cholestatic liver injury in the absence of prohibitin-1. *Hepatology* **62**, 1237–1248 (2015).